A transcriptomics-guided drug target discovery strategy identifies novel receptor ligands for lung regeneration

Xinhui Wu[1,2], I. Sophie T. Bos[1,2], Thomas M. Conlon[3], Meshal Ansari[3], Vicky Verschut[1,6] Lars A. Verkleij[1,2], Angela D'Ambrosi[1,2], Aleksey Matveyenko[4], Herbert B. Schiller[3], Melanie Königshoff[5], Martina Schmidt[1,2], Loes E. M. Kistemaker[1,2,6], Ali Önder Yildirim[3], Reinoud Gosens[1,2,*]

*[1]Department of Molecular Pharmacology, Faculty of Science and Engineering, University of Groningen, Antonius Deusinglaan 1, 9713AV, Groningen, The Netherlands, [2]Groningen Research Institute for Asthma and COPD, University Medical Center Groningen, University of Groningen, Groningen, The Netherlands, [3]Institute of Lung Biology and Disease (ILBD)/Comprehensive Pneumology Center (CPC), Helmholz Zentrum München, Munich, Germany, Member of the German Center for Lung Research (DZL), [4]Department of Physiology and Biomedical Engineering, Mayo Clinic Collage of Medicine, Rochester, Minnesota, USA, [5]University of Pittsburg, [6]Aquilo BV, Groningen, The Netherlands, *Correspondence*

Abstract

Currently, there is no pharmacological treatment targeting defective tissue repair in chronic disease. Here we utilized a transcriptomics-guided drug target discovery strategy using gene signatures of smoking-associated chronic obstructive pulmonary disease (COPD) and from mice chronically exposed to cigarette smoke, identifying druggable targets expressed in alveolar epithelial progenitors of which we screened the function in lung organoids. We found several drug targets with regenerative potential of which EP and IP prostanoid receptor ligands had the most significant therapeutic potential in restoring cigarette smoke-induced defects in alveolar epithelial progenitors *in vitro* and *in vivo*. Mechanistically, we discovered by using scRNA-sequencing analysis that circadian clock and cell cycle/apoptosis signaling pathways were enriched in alveolar epithelial progenitor cells in COPD patients and in a relevant model of COPD, which was prevented by PGE2 or PGI2 mimetics. Conclusively, specific targeting of EP and IP receptors offers therapeutic potential for injury to repair in COPD.

Key words: PGE2; PGI2; repair; cell cycle; circadian clock signaling; drug screening

Introduction

One of the main challenges in pharmacology today is the generation of drugs with regenerative potential, with the ability to restore tissue repair in chronic disease. Regenerative medicine has thus far mainly focused on transplantation, tissue engineering approaches, stem- or progenitor cell therapy, or a combination of these[1]. A regenerative pharmacological approach will have considerable additional potential because it can be applied on a relatively large scale. Furthermore, it can be used to halt the disease process in an early stage resulting in real disease-modifying treatment. Also, pharmacological targeting may aid or support other regenerative strategies.

There is a need for regenerative pharmacology in respiratory, cardiovascular, and neurological diseases as well as many other disease areas. In respiratory medicine, chronic obstructive pulmonary disease (COPD) is one of the most common lung diseases with a need for regenerative therapies. The disease is characterized by airflow limitation that is not fully reversible, and which deteriorates progressively. The main difficulty underlying COPD pathogenesis is increased tissue destruction in combination with abnormal tissue repair in susceptible individuals. As current therapies do not modify the course of the disease, developing new therapeutic strategies aiming at regeneration of tissue is necessary.

In affected individuals, there is an increase in alveolar air space associated with destruction of alveolar epithelial cells along with reduced capacity of epithelial progenitors to restore this defect. In the distal lung, alveolar type II cells and alveolar epithelial progenitors harbour stem cell capacity and function to maintain alveolar epithelium[2]. These cells reside in a local tissue microenvironment called the niche, which is composed of supporting cells such as fibroblasts and alveolar macrophages. The niche controls adequate activation of the progenitor cell[1–3] by means of secreted

64 factors such as WNTs, FGFs, retinoic acid, and many other factors that control
65 stemness, proliferation and differentiation[3].

66 Like in many chronic diseases associated with ageing, this local lung
67 microenvironment is insufficiently supportive for lung repair in COPD [1,4,5]. For example,
68 studies have indicated that an imbalance of canonical and noncanonical WNT
69 signaling results in impaired alveolar regeneration in COPD[4,6]. Moreover, lymphotoxin-
70 β (LTβ), released from CD8+ T-cells in COPD, can negatively interfere with repair.
71 LTβ induces noncanonical NFκB signalling, thereby repressing functional Wnt/β-
72 catenin signalling in the lung[5]. Accordingly, the challenge towards successful
73 regenerative pharmacology in COPD needs to take into consideration the specific
74 hostile microenvironment and the abnormal repair process that stands in the way of
75 adequate regeneration in COPD.

76 In the present study, we hypothesized that a transcriptomics guided drug target
77 discovery strategy based on gene signatures differentially expressed in COPD and in
78 response to cigarette smoke may be used to identify novel druggable gene targets
79 that are specifically involved in defective lung repair in COPD. Our results show that
80 such a strategy coupled to functional studies in organoids yields novel receptor ligands
81 of which EP and IP prostanoid receptor had the most significant potential in
82 counteracting the negative effects of cigarette smoke on alveolar progenitor cell
83 function.

84 ## Results

85 **Transcriptomics-guided screening to identify novel targets.** We set out to identify
86 novel drug targets that may help restore defective lung repair. To achieve this, we
87 utilized a transcriptomics-guided target discovery strategy (described in Fig. 1a) based
88 on gene signatures of COPD lung tissues [7] and of a relevant model of cigarette smoke

exposure[8] to identify differentially regulated druggable genes. We found Reactome pathways related to inflammation such as *Neutrophil degranulation* and *Innate immune system* as well as pathways related to the extracellular matrix such as *Extracellular matrix organization* and *Integrin cell surface interactions* to be enriched in both datasets (Fig. 1b-e). We identified 38 individual target genes that were concordantly up- and 30 individual target genes concordantly downregulated. These genes were filtered through the 'Drug-gene interactions and potential druggability in the drug gene interaction database' (DGIdb, http://www.dgidb.org/), which rendered 25 druggable upregulated genes and 16 druggable downregulated genes (Fig. 1f). Genes were further filtered for expression in lung epithelial cells or fibroblasts by consulting the human lung cell atlas (https://asthma.cellgeni.sanger.ac.uk/) and lung map (https://lungmap.net/), which yielded 15 druggable target genes.

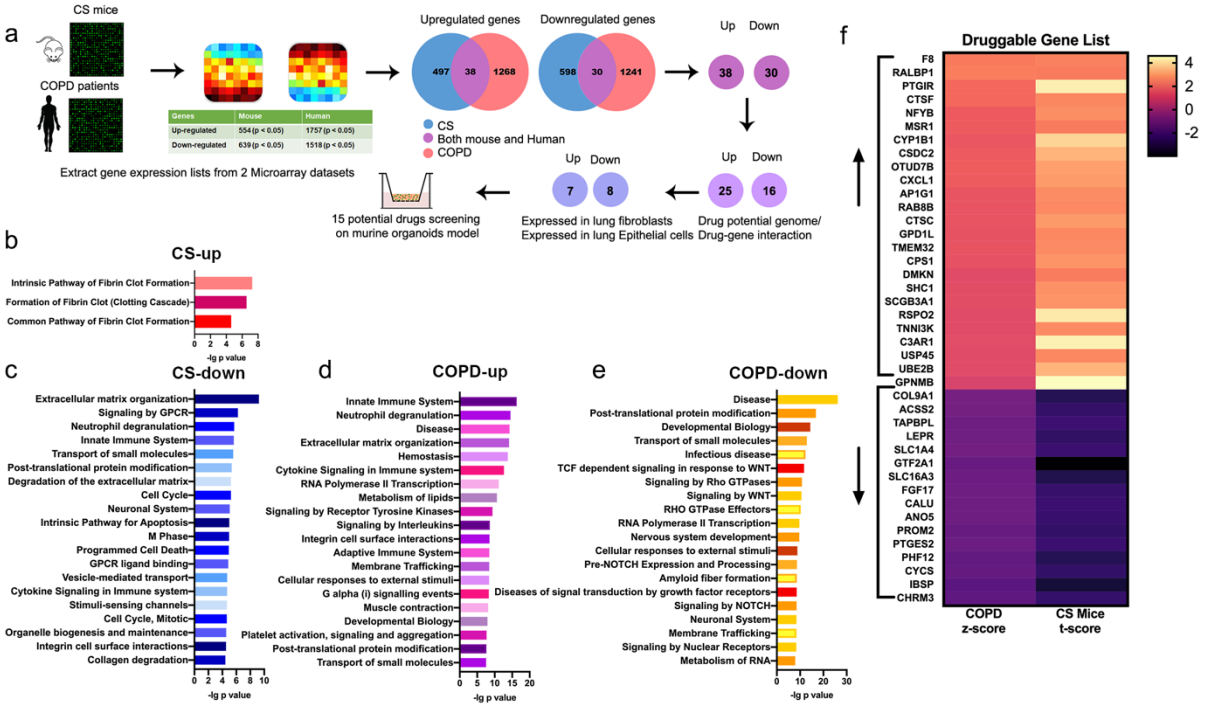

Figure 1 Overview of the transcriptomics-guided drug discovery strategy. a Schematic outline of the drug screening strategy. **b-c** Reactome pathway enrichment analysis of differentially up- and downregulated genes from CS-exposed mice[8] using GSEA (https://www.gsea-msigdb.org/gsea/msigdb/annotate.jsp). **d-e** Reactome pathway enrichment analysis of up- and

downregulated genes from COPD patients[7] using GSEA, the top 20 pathways enriched are presented. **f** Heatmap shows the gene expression pattern of the druggable genes (http://www.dgidb.org/) identified both in CS-exposed mice and COPD patient databases.

To assess the potential relevance of signaling functionally associated with the 15 genes of interest, we set up an *in vitro* organoid model to perform specific drug screening tests. We co-cultured human and mouse CD31-/CD45-/ EpCAM$^+$ lung epithelial cells with CCL206 lung fibroblasts in organoids in Matrigel and exposed these *in vitro* to different concentrations (1.25%, 2.5%, 5%) of cigarette smoke extract (CSE) (Fig. 2a, c). The number and size of organoids established by co-culturing human lung tissue derived CD31-/CD45-/EpCAM$^+$ cells and MRC5 fibroblasts was significantly decreased by CSE in a concentration dependent manner at day 14 (Fig. 2b). The total number of murine organoids quantified at day 14 of treatment with different concentrations of CSE yielded similar results and was decreased in a CSE dose dependent manner as well (Fig. 2e). To specifically analyze the impact of CSE on organoids derived from alveolar epithelial progenitors, we morphologically subclassified organoids into airway and alveolar type[9] organoids (Fig. 2d), which revealed that alveolar organoid numbers were more susceptible to cigarette smoke extract exposure than airway organoids (Fig. 2e). Immunofluorescence (IF) studies confirmed that the number of acetylated-α tubulin$^+$ (ACT; ciliated cell marker, airway type organoids) and pro-SPC$^+$ (type II cell marker, alveolar type organoids) organoids was significantly decreased by 5% CSE (Fig. 2f). The size of both organoid types was decreased at day 14 (Fig. 2g).

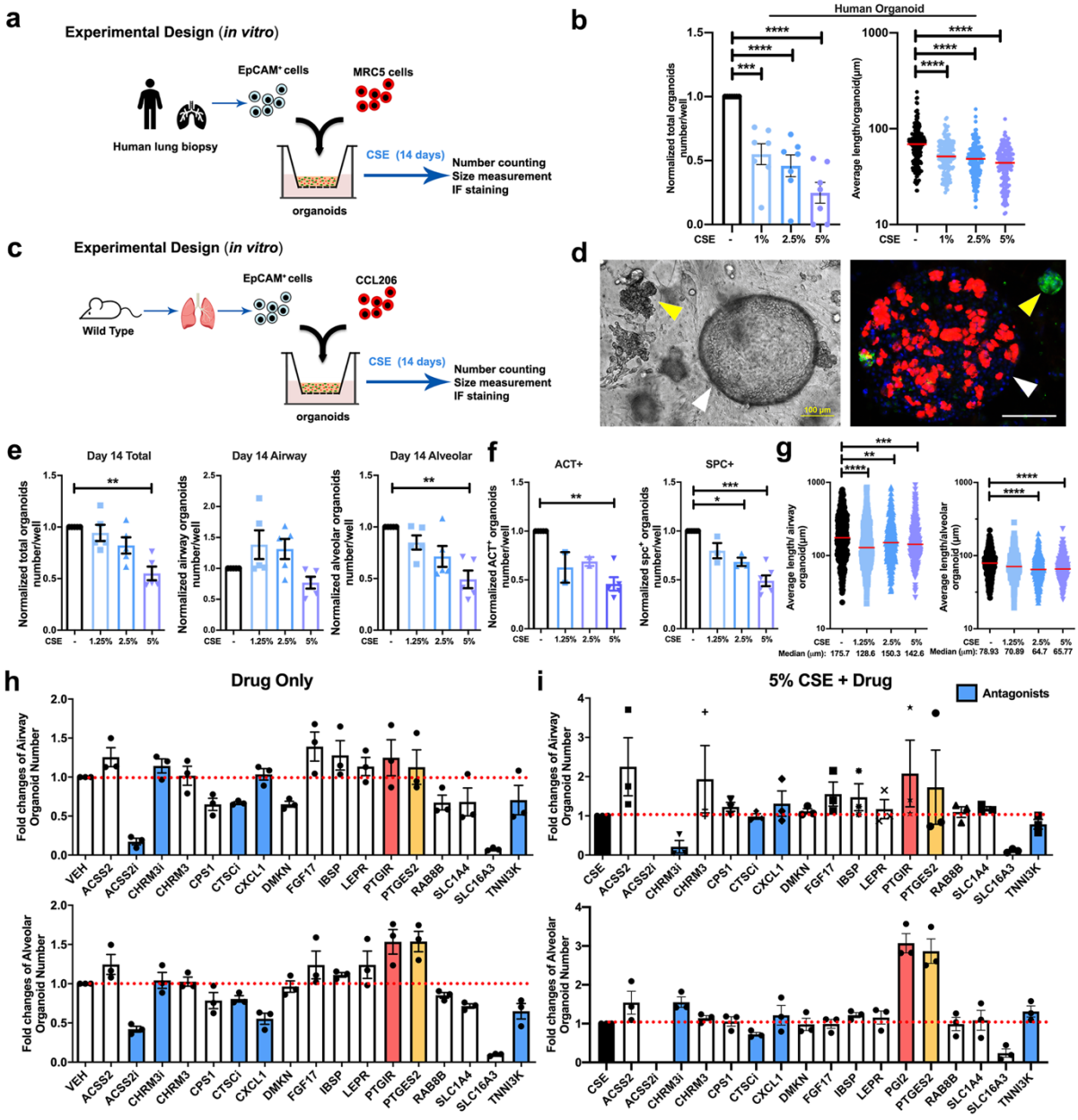

Figure 2. Cigarette smoke exposure represses adult epithelial lung organoid formation. a Schematic of *in vitro* human experimental design. **b** Quantification of total amount of human organoids and the quantification of average human organoid diameters after treatment with cigarette smoke extract (CSE) (0, 1, 2.5, and 5%). N = 7 experiments (2 healthy, 5 COPD donors). n > 150 organoids/group. **c** Schematic of *in vitro* murine experimental design. **d** Representative images of murine lung organoids. Left: light microscopy. Right: immunofluorescence of organoids. Green: pro-SPC (SPC), red: acetylated-α tubulin (ACT), blue: DAPI. White arrow: airway type of organoid, yellow arrow: alveolar type of organoid. Scale bar, 100 μm. **e** Quantification of the normalized number of total organoids, airway, and alveolar type organoids on day 14 obtained after treatment with different

concentrations of CSE (0, 1.25, 2.5, and 5%). **f** Quantification of normalized ACT$^+$ and pro-SPC$^+$ organoids obtained after treatment with 0, 1.25, 2.5, and 5% CSE. **g** Quantification of average organoid diameter after treatment with 0, 1.25, 2.5, and 5% CSE measured on day 14. N = 5 experiments, n > 380 organoids/group. **h-i** Overview of drug screening using the *in vitro* murine lung organoid model. Comparison of the normalized number of airway and alveolar type organoids treated with the different drugs of interest in the absence **(h)** or presence **(i)** of 5% CSE. Red bar: PTGIR, yellow bar: PTGES2, blue: antagonists. Data are presented as mean ± SEM in number quantification. Data are presented as scatter plots with medians in size quantification. For all panels: **p < 0.05, **p < 0.01, ***p < 0.001, ****p < 0.0001.

We next aimed to utilize this lung organoid model to evaluate the efficacy of existing COPD therapeutics. Increasing evidence[10,11] has linked phosphodiesterase (PDE) 4 inhibition to the therapeutic management of respiratory diseases, and roflumilast has been used as an oral medication in COPD patients with a prior history of hospitalization for an acute exacerbation (GOLD 2021). This led us to explore whether the classic PDE4 inhibitor, rolipram, was able to rescue the CS-induced reduction in organoid formation by alveolar progenitors. Thus, organoids were subjected *in vitro* to different concentrations (1 and 10 μM) of rolipram in the presence and absence of 5% CSE for up to 14 days (Fig.S1a). Rolipram (10 μM) alone significantly increased the total number of organoids at day 7 as well as the pro-SPC$^+$ organoids at day 14 (Fig.S1b, c), but had no beneficial effects on organoid numbers when combined with CSE exposures. Treatment with rolipram (1 μM) either alone or in combination with CSE induced significantly increase alveolar organoid size (Fig.S1d).

Budesonide is an inhaled corticosteroid used in COPD management[12–15]. Therefore, we examined its effect also in our *in vitro* (Fig. S1e) and *in vivo* (Fig. S1h) CS/organoid models. Intriguingly, budesonide (1-, 10-, 100 nM) in combination with CSE exposure further reduced the number as well as the size of both airway and alveolar type

organoids as compared to CSE exposure alone (Fig. S1f, g). *In vivo* exposure to budesonide together with CS increased the number of airway but not alveolar organoids (Fig. S1i), without affecting organoid size (Fig. S1j). Taken together, these data show that *in vitro* exposure to cigarette smoke extract functionally represses human alveolar epithelial progenitor organoid formation, resulting in reduced growth and differentiation, which can be mimicked using murine alveolar epithelial progenitors. Validating the limitations of current pharmacology, PDE4 inhibitors and corticosteroids do not prevent or reduce the detrimental effects of cigarette smoke on organoid formation.

The assay was used subsequently to screen for the functionality of the targets in restoring organoid growth. Genes downregulated in response to CS and COPD were targeted with activating ligands, whereas genes upregulated in response to CS and COPD were targeted using antagonists with exception of *ACSS2* and *CHRM3* for which we included both an agonist and an antagonist. The effects of the drugs targeting the 15 selected genes alone (compared to vehicle, Fig. 2h) and in the presence of 5% CSE exposure (Fig. 2i) on the number of organoids were determined. Specific information of all drug effects on organoid number and size are summarized in Supplementary figure 2 and 3. Interestingly, the compound activating ACSS2 (Acetyl-CoA synthetase short-chain family member 2), increased the number of airway type organoids and the size of alveolar organoids in combination with CSE (Fig. S2-3), whereas the ACSS2 inhibitor had the opposite effects. Atropine (CHRM3 antagonist), IBSP (Integrin Binding Sialoprotien) and LEPR (Leptin receptor) tended to increase the number and size of alveolar organoids in response to CSE as well (Fig. S2-3). However, considering the overall magnitude of alveolar type organoids particularly, PGE2 (target gene *PTGES*) and iloprost, (PGI2 analogue, target gene

190 *PTGIR*) were identified as the by far most promising targets with regards to their
191 capacity in restoring the CSE-induced repression of organoid formation (Fig. 2h-i, S2-
192 3).

193 **PGE2 and PGI2 significantly prevent alveolar epithelial dysfunction.** The
194 *PTGES2* and *PTGIR* genes encode membrane-associated prostaglandin E synthase
195 and the prostacyclin (PGI2) receptor, respectively. PGE2 acts on 4 receptor subtypes,
196 being *PTGER1-4*, whereas PGI2 acts primarily on *PTGIR*. We assessed their
197 expression in human lung tissue of healthy smokers and COPD patients and found
198 maintained expression of all receptors in disease with some small differences in
199 expression, most notably a reduced expression of *PTGER2* and increased expression
200 of *PTGIR* (Fig. 3a). Single cell RNAseq (sc-RNAseq) data from human lung tissue
201 shows similar expression of all 5 receptors was detected in alveolar epithelial cells and
202 in fibroblasts (http://www.copdcellatlas.com/). Single cell RNA sequencing of mouse
203 lung tissue showing that expression of *Ptger2* and *Ptger4* were highest compared to
204 that of *Ptger1* and *Ptger3* in mesenchymal cells (Fig. 3b, c). Interestingly, the
205 expression of *PTGES,* and *PTGES2*, the enzymes responsible for PGE2 synthesis
206 were relatively ubiquitous in human and mouse lung tissue, whereas *PTGIS*, the
207 enzyme responsible for PGI2 synthesis was highest in mesenchymal cell types
208 including fibroblasts. The expression of all these receptors showed lower copy
209 numbers, which is expected for G protein-coupled receptors (GPCRs).

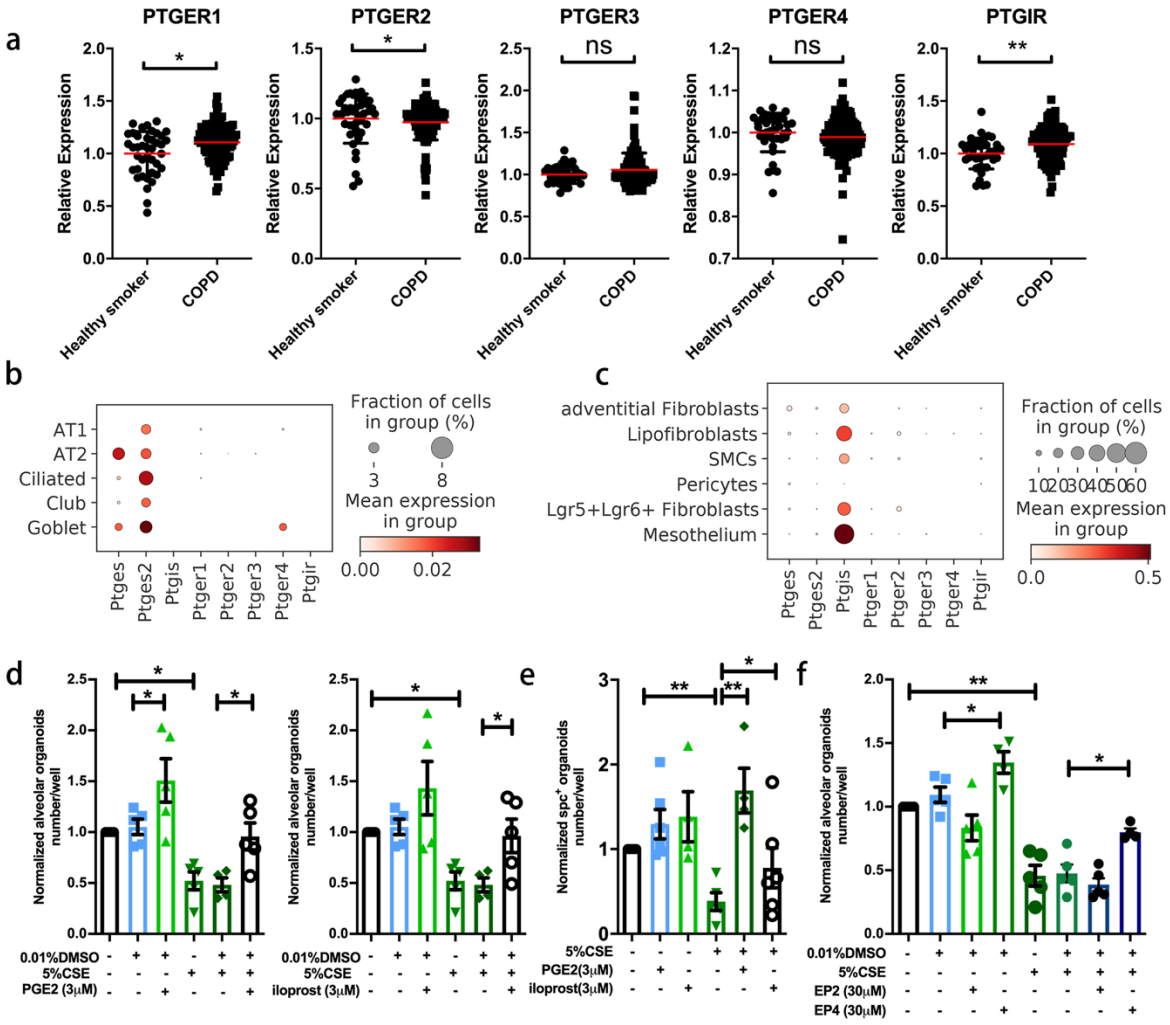

Figure 3 16,16-dimethyl prostaglandin E2, iloprost, and selective EP2 and EP4 analogues restore lung organoid formation in response to cigarette smoke (extract). a The relative gene expression of *PTGER1, PTGER2, PTGER3, PTGER4* and *PTGIR* in healthy smokers (N = 40) and COPD patients (N = 111) downloaded from the NCBI GEO database GSE76925. **b-c** Data are extracted from the NCBI GEO database GSE151674 **b** The expression *of Ptges, Ptges2, Ptgis, Ptger1, Ptger2, Ptger3, Ptger4* and *Ptgir* in epithelial cells using scRNA-seq analysis of mouse lung tissue. **c** The expression *of Ptges, Ptges2, Ptgis, Ptger1, Ptger2, Ptger3, Ptger4* and *Ptgir* in mesenchymal cells using scRNA-seq analysis of mouse lung tissue. **d** Quantification of normalized number of alveolar type organoids treated with vehicle control, or 5% CSE ± PGE2 agonist (16,16-dimethyl prostaglandin E2)/iloprost. **e** Quantification of normalized number of SPC^+ organoids treated with vehicle control, or 5% CSE ± PGE2 agonist (16,16-dimethyl prostaglandin E2) or iloprost. **f** Quantification of normalized number of alveolar type of organoids treated with vehicle control, or 5% CSE ± selective EP2 or EP4 agonist. Data are presented as mean ± SEM. *p < 0.05, **p < 0.01, ***p < 0.001, ****p < 0.0001.

To further characterize the effects of PGE2 and PGI2 on defective alveolar epithelial progenitors, we examined them *in vitro* (Fig. 3d-f) and *in vivo* (Fig. 4) CS(E). The PGE2 analogue 16,16-dimethyl prostaglandin E2 and the prostacyclin analogue iloprost both increased the number of alveolar type organoids even in the presence of 5% CSE (Fig. 3d) and significantly increased the number of SPC^+ organoids under conditions of CSE exposure (Fig. 3e). To address the relative roles of the two Gs-coupled PGE2 receptors, EP2 and EP4, we evaluated the selective agonists ((R)-Butaprost and 5-[(3S)-3-hydroxy-4-phenyl-1-buten-1-yl]1-[6-(2H-tetrazol-5R-yl)hexyl]-2-pyrrolidinone, CAY10598) of these receptors. Focus was on these Gs coupled receptors, as we found that cholera toxin, a well-known inducer of constitutive adenylyl cyclase activity and cAMP signaling, increased organoid formation both with and without the exposure to CSE (Fig. S4a). The EP2 selective butaprost had no effects on organoid number (Fig. 3f) but increased the alveolar size in the absence and presence of 5% CSE (Fig. S5c). The EP4 selective agonist increased the number of alveolar type organoids significantly and prevented the number reduction resulting from 5% CSE exposure (Fig. 3f). The EP4 agonist also increased the size of both types of organoids in the absence and presence of 5% CSE (Fig. S5c). To explore whether duration of drug exposure affected organoid formation, the organoids were treated *in vitro* with PGE2 analogue or PGI2 analogue for 3 different time windows during organoid development as illustrated in Supplementary figure 5d-g. These time windows were identified previously[9], and mark the initial division phase (day 0-2), proliferation (day 2-7), and differentiation phase (day 7-14). We observed no effects on the number of organoids for any of the short-term drug treatments, suggesting continuous treatment with or iloprost during all phases of organoid formation is required.

To examine the effects of PGE2 and PGI2 *in vivo*, we exposed mice to air (vehicle control), CS, CS + misoprostol (PGE2 analogue), or CS + iloprost as shown in Figure 4. To assess the impact of *in vivo* cigarette smoke (CS) exposure, we isolated CD31-/CD45-/EpCAM$^+$ cells from mice exposed to air or CS and co-cultured these with CCL206 fibroblasts *in vitro* for 14 days (Fig. 4a). Interestingly, the number of alveolar organoids was significantly decreased after *in vivo* CS exposure indicating that a relatively short exposure to cigarette smoke *in vivo* is sufficient to capture early changes in progenitor cell function (Fig. 4c). Cigarette smoke exposure did not change the yield of CD31-/CD45-/EpCAM$^+$ cells, whereas exposing mice to misoprostol or iloprost increased the yield of EpCAM+ cells (Fig. S6a). The organoid assay revealed that *in vivo* (i.p.) treatment with either misoprostol or iloprost significantly increased the number of alveolar type and SPC$^+$ organoids (Fig. 4e-f) *ex vivo*. Next, to investigate whether *in vitro* drug treatment would have similar effects on damage caused by *in vivo* CS exposure, we isolated EpCAM$^+$ cells from either air- or CS-exposed mice and subjected these to *in vitro* misoprostol or iloprost treatment in the organoid assay for 14 days (Fig. 4g). *In vitro* misoprostol increased the number of alveolar type organoids in cultures derived from CS-exposed mice (Fig. 4h). Only *in vitro* misoprostol increased the size of alveolar organoids derived from CS-exposed animals (Fig. S6c). Taken together, our data show that PGE2 and PGI2 analogues protect alveolar epithelial progenitor function from the effects of CS exposure. In addition, EP4 rather than EP2 seems to mediate the protective effects of PGE2.

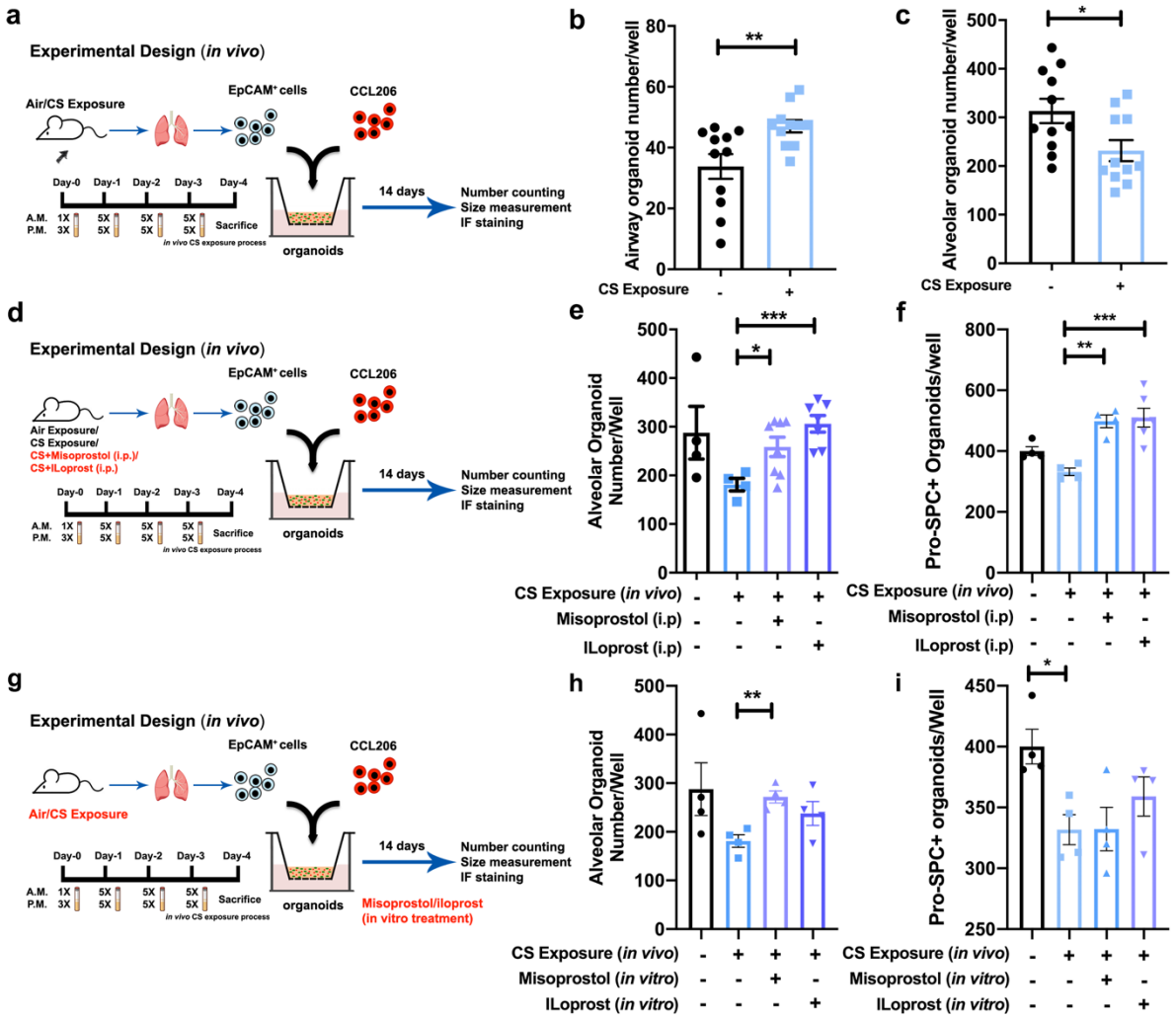

Figure 4 Administration (*in vivo* and *in vitro)* of misoprostol and iloprost to cigarette smoke-exposed mice restored lung organoid formation. a Schematic of *in vivo* CS exposure experimental setup. **b-c** Number of airway and alveolar type organoids quantified on day 14 of co-culturing CCL-206 fibroblasts and EpCAM$^+$ cells (isolated from air exposed/CS exposed mice). N = 11 experiments. **d** Schematic of experimental design. Organoids were generated from air- or CS-exposed mice treated *in vivo* with misoprostol (i.p.) or iloprost (i.p.); all organoids were treated with normal organoid medium. **e-f** Number of alveolar type and pro-SPC$^+$ organoids quantified on day 14 from co-culture of CCL-206 fibroblasts and EpCAM$^+$ cells (isolated from air- (control) and CS-exposed mice treated intraperitoneally with misoprostol or iloprost). **g** Schematic of experimental design. Organoids were generated from mice exposed to air or CS. Misoprostol and iloprost were added *in vitro* to the organoid medium for treatment. **h-i** Number of alveolar type and SPC$^+$ organoids quantified on day 14 from co-culture of CCL-206 fibroblasts and EpCAM$^+$ cells (isolated from air- and CS-exposed mice) treated with misoprostol/iloprost *in vitro*. Data are presented as mean ± SEM. *p < 0.05, **p < 0.01, ***p < 0.001, ****p < 0.0001.

Distinct genetic signatures in regulation of defective alveolar epithelial repair. To unravel the transcriptional changes leading to impaired lung organoid formation after exposure to CS as well as the mechanisms underlying the beneficial effects of PGE2 and PGI2 treatment, we performed RNA sequencing (Fig. 5a) on EpCAM^{+} cells isolated from mice exposed to air (control), CS, CS + misoprostol(i.p.), or CS + iloprost (i.p.), directly after the isolation procedure (i.e., prior to inclusion in the organoid assay). Principal-component analysis (PCA) revealed that the CS-exposed group is transcriptionally distinct from the control group (Fig. 5b), and that the CS/misoprostol and CS/iloprost groups are transcriptionally different from the CS exposed group. The top 20 differentially expressed genes from these three comparisons, including both up- and downregulated genes, are shown in the heatmaps (Fig. 5c) and summarized in supplementary materials. Reactome pathway analysis was used to identify molecular pathways overrepresented in CS/misoprostol/iloprost-modulated genes in alveolar epithelial cells. Within the top 20 enriched pathways (Fig. 5d, supplementary materials), genes associated with cell cycle, mitotic prometaphase, DNA replication/synthesis and RHO GTPases activate formins signaling pathways were upregulated by CS exposure compared to air (control) exposure, however, these were downregulated by treatment with misoprostol or iloprost. Notably, genes associated with the circadian clock signaling pathway were downregulated by CS exposure but restored by treatment with misoprostol or iloprost. Moreover, signaling by FGFR1, 3 and 4 were downregulated in response to CS exposure, whereas the same signaling pathways were upregulated by misoprostol but not iloprost treatment. These findings suggest that the repairing mechanisms of misoprostol and iloprost in response to CS were common in cell cycle and circadian clock signaling and the distorted FGFR signaling resulted from CS was corrected by misoprostol uniquely. In addition, the

nuclear receptor transcription pathway, growth hormone receptor signaling, MAPK, WNT and cell-cell communication signaling pathways appear to downregulate in response to CS, which were not observed in either misoprostol/iloprost treatment group. Overall, the RNA-seq analysis demonstrates both common and distinct transcriptomic mechanisms of misoprostol and iloprost treatment in response to CS exposure in alveolar epithelial progenitors.

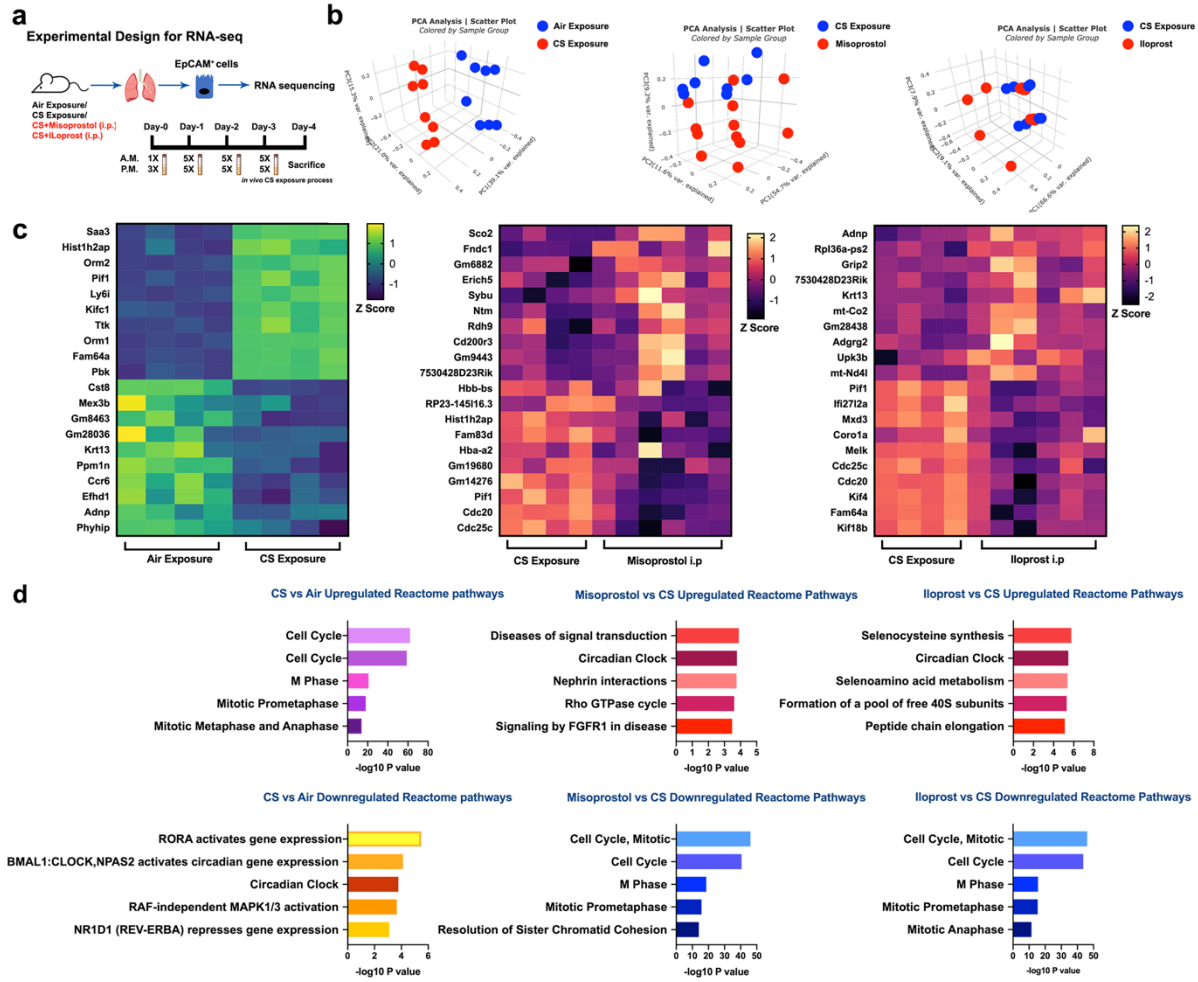

Figure 5 Transcriptomic signatures in response to cigarette smoke with(out) misoprostol and iloprost. a Schematic experimental design for RNA sequencing. **b** PCA plots demonstrate the clusters betweern different comparisons: air vs CS, CS vs CS+misoprostol, and CS vs CS+iloprost. **c** Heatmaps displaying the top 20 differentially expressed genes in air vs CS, CS vs CS+misoprostol, and CS+iloprost exposed epithelial cells. **d** The top 5 significantly up- and downregulated reactome

pathways enrichment form differentially expressed genes within the comparisons of air vs CS exposure, CS exposure vs CS+misoprostol, and CS exposure vs CS+iloprost.

Discussion

Chronic obstructive pulmonary disease results from repeated micro-injuries to the epithelium often caused by tobacco smoking. In susceptible individuals, this results in tissue remodeling in the conducting airways and destruction of the respiratory bronchioles and alveoli[19]. No clinically approved pharmacological treatment prevents or reverses the tissue destruction in the distal lung. The results of our study are in line with this contention and demonstrate that the PDE4 inhibitor rolipram and the corticosteroid budesonide had no, or only very limited, beneficial effects on impaired organoid growth and differentiation in response to cigarette smoke extract *in vitro* or in response to cigarette smoke exposure *in vivo*. In fact, if anything, budesonide appeared to restrict progenitor cell growth, which is a concern given the wide use of corticosteroids in the management of COPD. This underscores the need for novel drug targets.

Consequently, we set out to search for new potential drug targets for lung repair in COPD and identify EP and IP receptor agonists as two such potential targets, by utilizing a transcriptomics-guided drug discovery strategy. Both EP and IP receptor agonists were able to promote epithelial repair responses after exposure to cigarette smoke (extract). Whereas PGE2 and PGI2 showed the most profound changes, other methods including ACSS2 agonism, LEPR agonism and IBSP agonism yielded smaller effects. ACSS2 supports acetyl-CoA synthesis from acetate in the cytosol[20,21], and thereby plays an important role in lipid metabolism and in the regulation of histone acetylation in the nucleus during gene transcription. IBSP is a member of the small

integrin-binding ligand N-liked glycoprotein (SIBLING) family[22,23], which is associated with bone metastases of lung cancer[24]. LEPR (leptin receptor), is an adipocytokine that has a central role in regulating food intake and energy expenditure[25], but has also been linked to lung function decline in a population in COPD[26]. Nonetheless, among all the candidate targets, PGE2 (*PTGES2*) and PGI2 (*PTGIR*) analogues emerged as the most promising compounds among all drugs in the current study. Prostaglandins (PGs) are lipid mediators synthesized from arachidonic acid (AA) via the cyclooxygenase pathway, and include PGD2, PGI2, PGH2, PGE2 and PGF2α[27]. PGI2 signals via IP receptors to induce cAMP signaling, similar to EP4 receptors. We show EP4 receptors to have similar expression as in non-COPD controls, whereas IP receptors are expressed at higher levels in COPD patients indicating the expression of both receptors is maintained in disease.

We show that PGE2 agonists are beneficial in reducing CS-induced damage in alveolar epithelial progenitors. However, PGE2 has been reported as an unstable molecule with an extremely short half-life; therefore, targeting its receptors with specific more stable analogues may be a better alternative. PGE2 is the most widely produced PG in the human body and it signals via four specific G-protein-coupled receptors (EP1-4[28,29]). The interactions between PGE2 and EP receptors depend on tissue and cell type, specific receptor expression, and differences in binding affinities, leading to unique patterns of EP receptor activation[30]. PGE2 can stimulate cAMP production through EP2 and EP4 receptors, whereas EP3 activation results in decreased cAMP synthesis and EP1 stimulation is coupled to Gq-activation and (enhanced) Ca^{2+} signaling[27,30,31]. EP1 and EP3 receptors can mediate bronchoconstriction indirectly through activation of neural pathways[32], as a consequence non-selective PGE2 analogues are unsuitable as pulmonary drugs.

Therefore, we selected analogues of EP2 and EP4 to mimic effect of PGE2 in our organoid assay, and demonstrated that EP4 agonism showed beneficial effects against impaired organoid formation in response to (CS)E exposure. Targeting EP4 receptors is worthwhile investigating in more detail in the future, as the effects may surpass epithelial repair only. Additional beneficial effects of EP4 agonism in COPD may include bronchoprotection[33] and inhibition of inflammation[34], suggesting that EP4 agonism could unify several functional features that support the treatment of COPD, making this an intriguing pharmacological target.

Iloprost, a stable PGI2 analogue [27,35–39], has been shown to have anti-inflammatory effects and protects against bleomycin-induced pulmonary fibrosis in mice[36], and is also clinically used for the treatment of pulmonary hypertension[35]. Although a recent study[38] showed iloprost improved clinical outcomes in COPD patients with poor lung oxygenation, its impact on alveolar repair is unknown. Here we show that iloprost prevents the repressed organoid formation resulting from CS(E) exposure.

By generating transcriptomic signatures of epithelial progenitors derived from mice exposed *in vivo* to air, CS, CS + misoprostol or CS + iloprost, we uncovered dynamic molecular signaling pathways in response to CS exposure. Intriguingly, we identified circadian clock signaling as being significantly repressed in the alveolar epithelial progenitors derived from mice exposed to CS, which could be improved by either misoprostol or iloprost treatment. Circadian rhythms[40–43] are normally generated and regulated by clock genes, including *BMAL1* (*ARNTL1*) and *CLOCK* encoding activators, period (*PER1-3*) and cryptochrome genes (*CRY1-2*) that encode repressors, and the nuclear receptors Rev-erb (*NR1D1* and *NR1D2*) and *RORA* which constitute secondary regulatory loops. These core clock genes not only activate or repress a cell-autonomous clock, but also regulate the clock-controlled genes

(CCGs)[44], thus interacting with other molecular signaling pathways. Previously, it has been demonstrated that clock signaling is downregulated in CS exposed mice, linked to an impairment of anti-oxidant defense mechanisms[45] and Rev-erbα has been shown as an key regulator of inflammatory response in lung injury models[16–18,46]

Furthermore, we found that CS exposure upregulated pathways associated with cell cycle activity in alveolar epithelial progenitors, which could be counteracted by *in vivo* misoprostol or iloprost treatment. The cell cycle[47–51] is driven by a set of tightly regulated molecular events controlling DNA replication and mitosis with four phases, and each individual cell may require different triggers in order to decide whether to enter proliferation or apoptosis. To further assess alveolar epithelial progenitors under which cell cycle/apoptotic status in response to CS exposure as well as additional PGE2/PGI2 treatments may be the next step to investigate in the future. A link between circadian clock and cell cycle signaling pathways has been proposed[44,50,52]. Importantly, the molecular control of the biological clock is dependent on cAMP signaling and cAMP activators are known to entrain the biological clock[53], explaining the link between PGE2 and PGI2 activation and restoration of the defective clock signaling in combination with CS exposure. Hence, it is of great interest to determine in more molecular detail how these two oscillatory systems communicate in regulating PGE2/PGI2-mediated lung repair in future studies.

In conclusion, in this study we demonstrate for the first time the protective effects of several drug candidates, and in particular PGE2 and PGI2 analogues, against *in vivo* and *in vitro* CS(E)-induced damage of alveolar epithelial progenitors. Furthermore, using transcriptome analysis, we show that CS induces a wide range of transcriptional changes, including alterations of circadian clock and cell cycle signaling pathways, which can be counteracted by either misoprostol (PGE2) or iloprost (PGI2) treatment.

Overall, these data provide promising therapeutic strategies to specifically address defective lung repair in respiratory diseases, in particular targeting EP4 and IP receptors.

Methods

Animals. All mouse experiments for organoid study were performed at the Central Animal Facility (CDP) of the University Medical Center Groningen (UMCG) in accordance with the national guidelines and upon approval of the experimental procedures by CDP and the Institutional Animal Care and Use Committee (IACUC) of the University of Groningen (CCD license AVD105002015303). C57BL/6J (555) and BALB/cByJ (Jax-strain) mice (both genders, 8–12 weeks of age) were maintained under 12-h light/ dark cycles and were allowed food and water ad libitum. Animals for circadian clock studies were exposed to CS and/or administrated with compounds at the same time of the day for all mice in all groups. Animals were euthanized at the same time of the day. Adult (female, 8-10 weeks of age) C57BL/6N mice were obtained from Charles River (Sulzfeld, Germany) for the single cell RNAseq analysis of lungs following exposure to chronic CS. These experiments were performed at the Helmholtz Zentrum München and approved by the ethics committee for animal welfare of the local government for the administrative region of Upper Bavaria (Regierungspräsidium Oberbayern) and were conducted under strict governmental and international guidelines in accordance with EU Directive 2010/63/EU.

Human material. The human lung tissue was obtained from lung transplant donors according to the Eurotransplant guidelines including the absence of primary lung diseases such as asthma and COPD, and no more than 20 pack years of smoking history[54]. Gene expression in human lung published data sets was obtained by down loading series matrix files from the NCBI GEO database for GSE76925[55] and gene expression normalized to healthy smokers.

448 ***In vivo* cigarette smoke exposure.** Mice (n = 4–11/group, 10-12 weeks old) were
449 exposed (whole body) to 3R4F research cigarettes (Tobacco Research Institute,
450 University of Kentucky, Lexington, KY) for four consecutive days (two sessions/day, 8
451 hours between each exposure) to establish an acute smoke-induced inflammation
452 model, as described previously[8]. In the cigarette smoke (CS) group, mice were
453 exposed to 1 cigarette in the morning and 3 in the afternoon on day 1. From day 2 to
454 4, mice were exposed to 5 cigarettes each session. All cigarettes were smoked without
455 a filter in 5 min at a rate of 5L/h in a ratio with 60 L/h air using a peristaltic pump (45
456 rpm, Watson Marlow 323 E/D, Rotterdam, NL). In the control group, mice were
457 exposed to fresh air using similar exposure chambers as the CS group.
458 In some studies, budesonide was nebulized (0.1 mM, 15 min/mouse/exposure) to
459 wild-type mice (n = 6) prior to each CS exposure. In separate studies, intraperitoneal
460 (IP) injections of 50 μg misoprostol or 50 μg iloprost were given 30 min to wild-type
461 mice (n = 6-8) prior to each CS exposure. On day 5, mice were sacrificed, and the
462 lungs were immediately used for establishing organoid cultures or stored at - 80°C for
463 further experimental uses.
464 For the single cell RNAseq analysis of lungs CS was generated from 3R4F
465 Research Cigarettes with the filters removed. Mice were whole body exposed to active
466 100% mainstream CS of 500 mg/m^3 total particulate matter (TPM) for 50 min twice per
467 day for 4m in a manner mimicking natural human smoking habits as previously
468 described[55]
469
470 **Fibroblast culture.** Mouse fibroblasts, CCL206 (Mlg [CCL206], ATCC, Wesel,
471 Germany) were cultured in DMEM/F12 medium supplemented with 10% (v/v) fetal
472 bovine serum, 100 U/mL penicillin/streptomycin, 2 mM L-glutamine, and 1%

amphotericin B in a humidified atmosphere under 5% CO_2/95% air at 37°C, as previously described[6,9,56]. For organoid experiments, fibroblasts were proliferation-inactivated by incubation in mitomycin C (10 µg/mL, Sigma, M4287) for 2 h, followed by 3 washes with PBS after which the cells were trypsinized before introduction into the organoid co-cultures. Human lung fibroblasts MRC5 (CCL-171; ATCC, Wesel, Germany) were cultured in Ham's F12 medium supplemented with the same additives as the murine fibroblasts medium.

Cigarette smoke extract (CSE). The smoke of two 3R4F research cigarettes was pumped into 25 mL warm fibroblasts culture medium to produce 100% cigarette smoke extract (CSE)[11]. All cigarettes were without a filter and smoke was passed through the medium using a peristaltic pump (45 rpm, Watson Marlow 323 E/D, Rotterdam, NL). CSE was freshly prepared before each set of experiments.

Organoid culture. The organoid culture system is based on previously published protocols from our group[6,9,56]. In brief, epithelial cells ($CD31^-/CD45^-/CD326^+$) were freshly isolated from murine or human lung tissue and co-cultured with murine CCL206 or human MRC5 fibroblasts, respectively, in Matrigel® (Corning Life Sciences B.V., Amsterdam, The Netherlands). $EpCAM^+$ ($CD31^-/CD45^-/CD326^+$) cells were isolated from mouse lung tissue (without the trachea) using the QuadroMACS™ Separator and antibody-bound magnetic beads (Miltenyi Biotec, Leiden, The Netherlands). $EpCAM^+$ cells and fibroblasts were mixed 1:1 (20,000 cells each) and suspended in 100 µL of Matrigel prediluted 1:1 (v/v) with DMEM supplemented with 10% FBS. This mixture of cells was added to a 24-well Falcon® cell culture insert (Corning, USA) within a 24-well plate containing 400 µL of organoid media (DMEM/F-12 supplemented with 5%

FBS, 1% penicillin/streptomycin, 1% glutamine, 1% amphotericin B, 0.025‰ EGF, 1% insulin-transferrin-selenium, and 1.75‰ bovine pituitary extract) underneath the insert in each well. Adult human donor tissue was isolated from histologically normal regions of lung tissue specimens obtained at University Medical Centre Groningen (Groningen, The Netherlands) from n = 7 patients (2 non-COPD and 5 COPD patients). Human lung tissues were incubated and homogenized overnight in an enzyme mixture at 4 °C; the $EpCAM^+$ isolation process was similar to that described above for murine lung tissue. Organoids were cultured in a humidified atmosphere under 5% CO_2/95% air at 37 °C and medium in the wells was refreshed every 2–3 days. To quantify the number of organoids, light microscopy at 20x magnification was used and organoids were counted manually. The diameter of the organoids (organoid size) was measured using NIS-Elements software with a light microscope.

For *in vitro* organoid experiments, organoids were continuously treated with control, 1.25% (1% for human organoids), 2.5% or 5% CSE and organoid culture medium was refreshed every other day. All information on the pharmacological compounds used in this study is provided in the Supplementary table 1.

Immunofluorescence staining. The immunofluorescence staining assay for organoids was performed as described previously by our group with minor modifications[6,9,56]. Organoids were fixed in acetone diluted 1:1 (v/v) with methanol for 15 min at –20 °C. After fixation, one mL of PBS with 0.02 % sodium azide was added to the well underneath the insert. Organoids were kept at 4°C for one week after fixation. BSA media was added on top of the insert for blocking at room temperature (RT) for 2h. Afterwards, primary antibody incubation was performed in PBS buffer with 0.1% BSA and 0.1% Triton X-100 overnight at 4 °C. The next day, the organoids were

washed with PBS for 30 min three times and secondary antibody incubation was performed for 2h at RT. After washing with PBS for 15 min, the organoids on the insert membrane were transferred to a glass slide with two drops of mounting medium containing DAPI (Abcam 104139, Cambridge, UK), and a coverslip was applied.

The slides were kept at 4 °C. Confocal images were acquired using a Leica SP8 microscope or a Leica DM4000B microscope. Images were obtained and analyzed with LASX (Leica) software (open resource, Leica Microsystems GmbH, Wetzlar, Germany).

RNA extraction and RNA sequencing (RNA-seq) analysis. The EpCAM$^+$ cells isolated from mice exposed to Air, CS, CS+misoprostol, or CS+iloprost were used to extract total RNA for RNA sequencing using NucleoSpin® RNA kit (Machery-Nagel, 740955, Germany) according to the manufacturer's instructions. RNA concentrations and qualities were analyzed using Nanodrop spectrophotometer. An Illumina NovaSeq 6000 sequencer was used for RNA-seq data analysis by GenomeScan (https://www.genomescan.nl). The procedure included data quality control, adapter trimming, alignment of short reads and feature counting. Library preparation was checked by calculating ribosomal (and globin) content. Checks for possible sample and barcode contamination were performed and a set of standard quality metrics for the raw data set was determined using quality control tools (FstQC v0.34 and FastQA). Prior to alignment, the reads were trimmed for adapter sequences using Trimmomatic v0.30. To align the reads of each sample, the ensemble mouse reference GRCm38 (patch 6) was used. Data analyses following the RNA-seq studies were performed using the BioJupies platform (https://amp.pharm.mssm.edu/biojupies/)[57]. Gene

expression in murine lung published data sets was obtained by downloading series matrix files from the NCBI GEO database GSE151674.

Statistics analysis. All data are presented as mean ± SEM unless indicated otherwise. Unless stated otherwise, all data were assessed for statistical significance using two-tailed Student's t-test or one-way ANOVA. The p-value indicating statistically significant differences between the mean/median values are defined as follows: *p < 0.05, **p < 0.01, ***p < 0.001, ****p < 0.0001. Statistical analyses were performed with GraphPad Prism 8 software.

Acknowledgements:

The authors would like to acknowledge the support from the Lung foundation Netherlands (Longfonds, grant 5.1.17.166) and China Scholarship Council (CSC201707720065).

Author Contributions:

Author X.W., R.G. conceptualized the project, analyzed and interpreted the data; R.G., L.E.M.K., and M.S. supervised the project; X.W., A.M., M.K., L.E.M.K., A.Ö.Y., and R.G. assisted designing the experiments; X.W., S.B., V.V., L.A.V., and A.D'M. performed the experiments; X.W., T.M.C., and M.A. prepared the figures; T.M.C., M.A., H.B.S., and A.Ö.Y. assisted in bioinformatics analysis; X.W., and R.G. wrote the manuscript; All authors reviewed and commented on the manuscript and agreed to the final version.

Competing interest:

Author V.V. and L.E.M.K. are employees of Aquilo BV. Author R.G. and M.K. are members of the BREATH consortium funded by the Lung foundation Netherlands (Longfonds). All other authors declare no competing interests.

Supplementary tables and figures

Supplementary Table 1 Information of final drug lists screened on organoid assay.

NO	Overlap Up	Full name	Drug/compound name	Final concentrations	Article No.	Company
1	CPS1	Carbamoyl-phosphate synthase 1	N-Acetyl-L-glutamic acid	10 μM	855642-25G	Sigma-Aldrich
2	CTSC	Cathepsin C/Dipeptidyl peptidase 1	Cathepsin c inhibitor	1 μM	BI-9740	Boehringer Ingelheim
3	CXCL1	C-X-C Motif Chemokine Ligand 1	Reparixin (L-Lysine salt)	100 nM	Cayman - 21492	Cayman chemical
4	DMKN	Derrmokine	Dermokine beta recombinant protein antigen	100 ng/mL	NBP1-86840PEP	Novus Biologicals
5	PTGIR	Prostaglandin I2 Receptor	iloprost	0.03-, 0.3-, 3 μM	SML1651	Sigma-Aldrich
6	RAB8B	RAB8B, Member RAS Oncogene Family	CHEMBL384759/Guranosine 5'-diphosphate sodium salt (GDP)	10 μM	G7127	Sigma-Aldrich
7	TNNI3K	TNNI3 Interacting Kinase	GSK-114	10 μM		
NO	**Overlap Down**	**Full name**	**Drug/compound name**		**Article No.**	**Company**
1	ACSS2	Acyl-CoA Synthetase Short Chain Family Member	Acetyl coenzyme A sodium salt	10 mM	A2056-1MG	Sigma-Aldrich
2	ACSS2i	2	ACSS2 inhibitor	10 mM	S8588	Selleckchem.com
3	CHRM3	Cholinergic Receptor Muscarinic 3	Methacoline	10 μM	A2251	Sigma-Aldrich
4	CHRM3i		Atrophine	1 μM	A0132	Sigma-Aldrich
5	FGF17	Fibroblast Growth Factor 17	Recombinant human FGF-17 protein	10 ng/mL	319-FG-025	R&D systems
6	IBSP	Integrin Binding Sialoprotein	Recombinant Human IBSP/Sialoprotein II Protein, CF	10 ng/mL	4014-SP-050	R&D systems
7	LEPR	Leptin Receptor	Recombinant Mouse Leptin Protein, CF	100 ng/mL	L4146-1MG	Sigma-Aldrich
8	PTGES2	Prostaglandin E Synthase 2	16,16-dimethyl Prostaglandin E2	0.03-, 0.3-, 3 μM	D0160	Sigma-Aldrich
			Misoprostol	3 μM	M6807	Sigma-Aldrich
9	SLC16A3	Solute Carrier Family 16 Member 3	Streptozocin	10 μM	S0130-50MG	Sigma-Aldrich
10	SLC1A4	Solute Carrier Family 1 Member 4	L-Alanine	100 μM	A7627-1G	Sigma-Aldrich

Supplementary Table 2 Information of compounds used in organoid assay.

Name	Final concentrations	Article No.	Company
Rolipram	1-, 10 μM	R6520	Sigma-Aldrich
Budesonide	1-, 10-, 100 nM	B7777	Sigma-Aldrich
Cholera toxin	0.1 mg/mL	C8052	Sigma-Aldrich
(R) -Butaprost (EP2 analogue)	30 μM	B6309	Sigma-Aldrich
EP4 analogue*	30 μM	CAY10598	Cayman chemical
Forskolin	10 μM	F6886	Sigma-Aldrich
IBMX (3-Isobutyl-1-methylxanthine)	100 μM	Obtained from AppliChem (Germany)	
db-cAMP (Bucladesine)	100 μM	D0627	Sigma-Aldrich
Olodaterol	100 nM	Obtained from AppliChem (Germany)	

*EP4 analouge: 5-[(3S)-3-hydroxy-4-phenyl-1-buten-1-yl]1-[6-(2H-tetrazol-5R-yl)hexyl]-2-pyrrolidinone

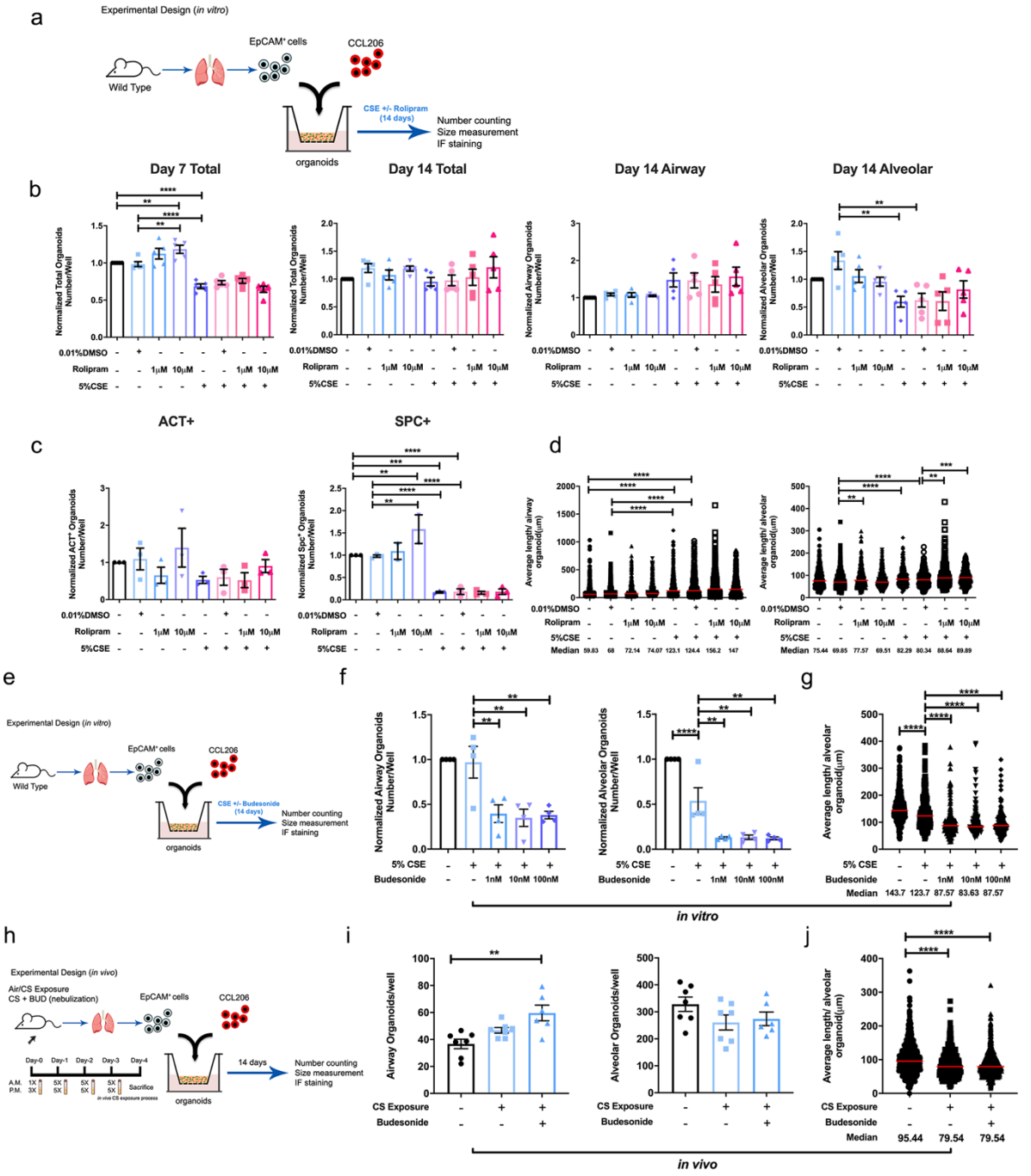

Supplementary figure 1. Effect of Rolipram and Budesonide on lung organoid formation.

a Schematic of *in vitro* experimental design. **b** Quantification of normalized number of total organoids (day 7), total organoids (day 14), airway type organoids (day 14), alveolar type organoids (day 14) treated with 5% CSE ± rolipram (0-, 1-, 10μM). **c** Quantification of normalized ACT$^+$ and SPC$^+$ organoid numbers treated with 5% CSE ± rolipram (0-, 1-, 10μM) at Day 14. **d** Quantification of average length (diameter) of airway and alveolar type organoids treated with 5% CSE ± rolipram (0-, 1-, 10μM) measured on day 14. N = 5 experiments, n > 503 organoids/group. Data are presented as scatter plots

with medians. **e** Schematic of *in vitro* experimental design. **f** Quantification of normalized number of airway and alveolar type organoids treated with 5% CSE ± Budesonide (0-, 1-, 10-, 100 nM) measured on day 14. **g** Quantification of average length (diameter) of alveolar type organoids (median value) treated with 5% CSE ± Budesonide (0-, 1-, 10-, 100 nM) measured on day 14. N = 4 experiments, n > 165 organoids/group. Data are presented as scatter plots with medians. **h** Schematic of *in vivo* experimental design. **i** Number of airway and alveolar type organoids from co-culture of CCL-206 fibroblasts and $EpCAM^+$ cells (isolated from air-exposed, CS-exposed, and CS-exposed + Budesonide nebulized mice) quantified on day 14. **j** Quantification of average length (diameter) of alveolar organoids (median value) from co-culture of CCL-206 fibroblasts and $EpCAM^+$ cells (isolated from air-exposed, CS-exposed, and CS-exposed + Budesonide nebulized mice) on day 14. N = 6 - 7 experiments, n > 671 organoids/group. Data are presented as scatter plots with medians. **p < 0.05, **p < 0.01, ***p < 0.001, ****p < 0.0001

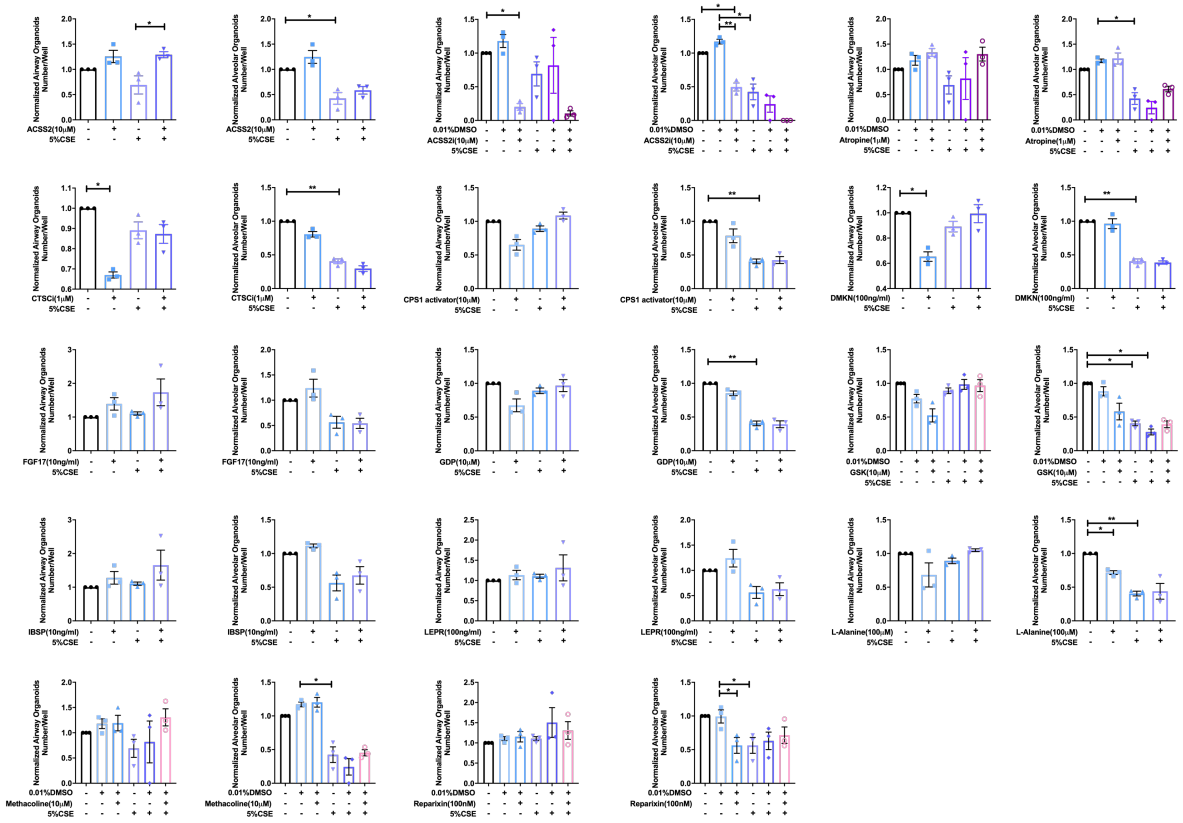

Supplementary figure 2 Effects of 15 drugs candidates of interest (including an additional agonist and antagonist for one gene target) on the normalized number of airway and alveolar type lung organoids in the presence and absence of 5% CSE. Data are presented as median ± SEM. **p < 0.05, **p < 0.01, ***p < 0.001, ****p < 0.0001.

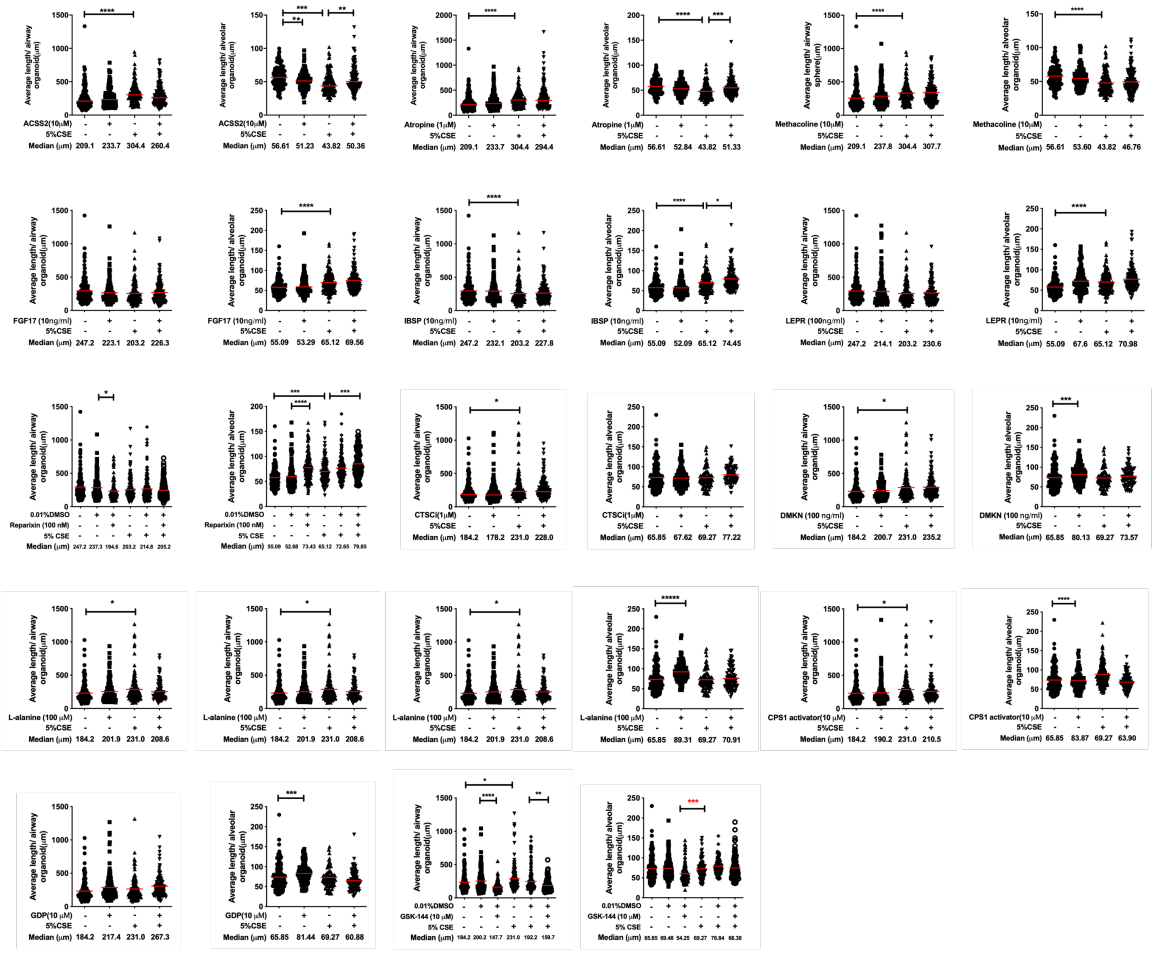

604

605 **Supplementary figure 3** Effects of 15 drugs candidates of interest (including an additional agonist and
606 antagonist for one gene target) on the size of airway and alveolar type lung organoids in the presence
607 and absence of 5% CSE. Data are presented as median ± SEM. **p < 0.05, **p < 0.01, ***p < 0.001,
608 ****p < 0.0001.

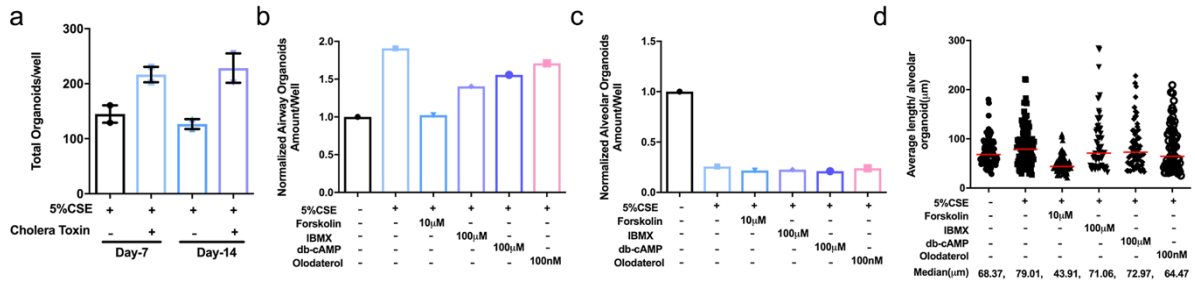

609

610 **Supplementary figure 4 Compounds related to cAMP signaling pathways tested on lung**
611 **organoid assay. a** Quantification of total organoids treated with 5% CSE + cholera toxin at different
612 time points. **b** Quantification of normalized airway type organoids treated with 5% CSE ± Forskolin (10
613 μM), IBMX (100 μM), db-cAMP (100 μM), and olodaterol (100 nM). **c** Quantification of normalized
614 alveolar type organoids treated with 5% CSE ± Forskolin (10 μM), IBMX (100 μM), db-cAMP (100 μM),

615 and olodaterol (100 nM). **d** Quantification of average length (diameter) of alveolar type organoids
616 (median value) treated with 5% CSE ± Forskolin (10 μM), IBMX (100 μM), db-cAMP (100 μM), and
617 olodaterol (100 nM). Data are presented as median ± SEM. **p < 0.05, **p < 0.01, ***p < 0.001, ****p
618 < 0.0001
619

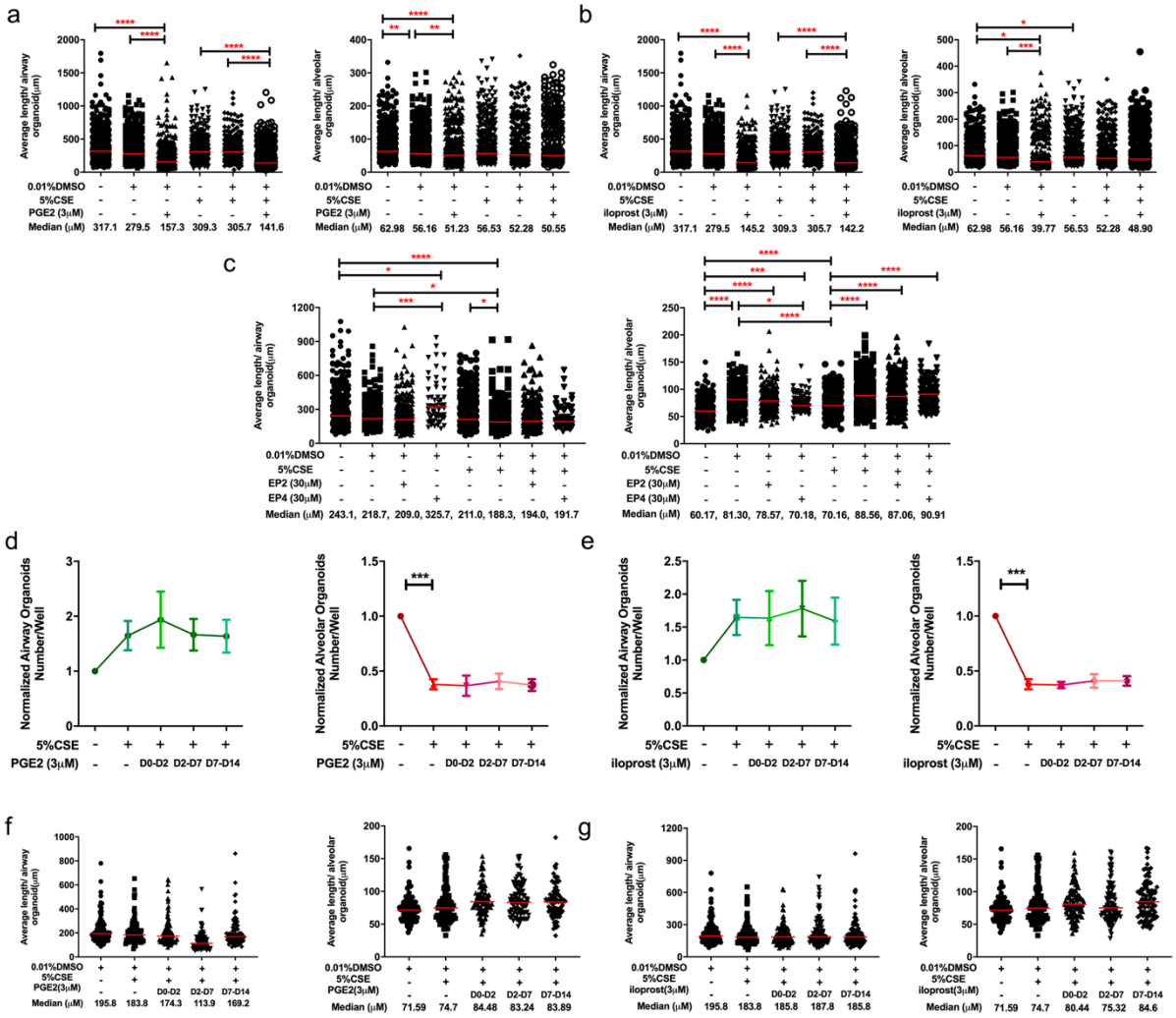

Supplementary figure 5 Quantification of lung organoid numbers and sizes in the study of PGE2/PGI2/EP2/EP4. a-b Quantification of average length (diameter) of organoids (median value) of airway and alveolar type organoids treated with 5% CSE ± PGE2 agonist (a)/iloprost (b) measured on day 14. N = 5 experiments, n > 334 organoids/group. Data are presented as median ± SEM. **c** Quantification of average length (diameter) of airway and alveolar type organoids (median value) treated with 5% CSE ± EP2/EP4 agonists measured on day 14. N = 5 experiments, n > 264 organoids/group. Data are presented as median ± SEM. **d-e** Quantification of normalized number of airway and alveolar type organoids treated with vehicle control, 5% CSE ± PGE2 agonist (d)/ iloprost (e) from day 0-2, day 2-7, or day 7-14. **f-g** Quantification of average length (diameter) of airway and alveolar type organoids (median value) treated with 5% CSE ± PGE2 agonist (f)/ iloprost (g) from day

0-2, day 2-7, and day 7-14. N = 2 experiments, n > 85 organoids/group. Data are presented as median ± SEM.

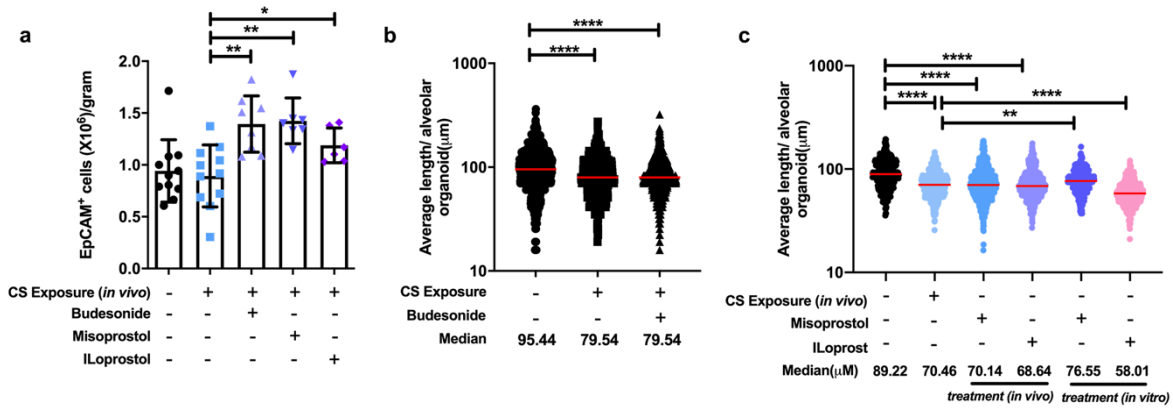

Supplementary figure 6 Quantification analysis of lung organoid assay in the *in vivo* study of PGE2/PGI2/Budesonide. a Yield efficiency of EpCAM$^+$ cells from mice with different treatments. **b** Quantification of average length of alveolar type organoids co-cultured from CCL-206 and EpCAM$^+$ cells isolated from air- (control) or CS-exposed mice with or without *in vivo* treatment with misoprostol or iloprost (i.p injection). N = 4-8 experiments, n = 400 organoids/group. **c** Quantification of average length of alveolar type organoids co-cultured from CCL-206 and EpCAM$^+$ cells isolated from air- or CS-exposed mice. Organoids were treated *in vitro* with misoprostol or iloprost for 14 days. N = 4-8 experiments, n = 400 organoids/group. Data are presented as median ± SEM. **p < 0.05, **p < 0.01, ***p < 0.001, ****p < 0.0001.

References

1. Kokturk, N., Yıldırım, F., Gülhan, P. Y. & Oh, Y. M. Stem cell therapy in chronic obstructive pulmonary disease. How far is it to the clinic? *Am. J. Stem Cells* **7**, 56–71 (2018).
2. Basil, M. C. *et al.* The Cellular and Physiological Basis for Lung Repair and Regeneration: Past, Present, and Future. *Cell Stem Cell* **26**, 482–502 (2020).
3. Volckaert, T. *et al.* Fgf10-Hippo Epithelial-Mesenchymal Crosstalk Maintains and Recruits Lung Basal Stem Cells. *Dev. Cell* **43**, 48-59.e5 (2017).
4. Hu, Y. *et al.* Wnt/β-catenin signaling is critical for regenerative potential of distal lung epithelial progenitor cells in homeostasis and emphysema. *Stem Cells* **38** (11) 1467-1478 (2020).
5. Conlon, T. M. *et al.* Inhibition of LTβR signalling activates WNT-induced regeneration in lung. *Nature* **588**, 151–156 (2020).
6. Wu *et al.* Mesenchymal WNT-5A/5B Signaling Represses Lung Alveolar Epithelial Progenitors. *Cells* **8** (10), 1147 (2019).
7. Brandsma, C. A. *et al.* A large lung gene expression study identifying fibulin-5 as a novel player in tissue repair in COPD. *Thorax* **70**, 21–32 (2015).
8. Kistemaker, L. E. M. *et al.* Muscarinic M3 receptors on structural cells regulate cigarette smoke-induced neutrophilic airway inflammation in mice. *Am. J. Physiol. - Lung Cell. Mol. Physiol.* **308**, L96–L103 (2015).
9. Ng-Blichfeldt, J. P. *et al.* Retinoic acid signaling balances adult distal lung epithelial progenitor cell growth and differentiation. *EBioMedicine **36**, 461-474* (2018).
10. Woodby, B. *et al.* The PDE4 inhibitor CHF6001 affects keratinocyte proliferation via cellular redox pathways. *Arch. Biochem. Biophys.* **685**, 1–8

(2020).

11. Zuo, H. *et al.* Cigarette smoke up-regulates PDE3 and PDE4 to decrease cAMP in airway cells. *Br. J. Pharmacol.* **175**, 2988–3006 (2018).

12. Kothe, T. B. *et al.* Surfactant and budesonide for respiratory distress syndrome: an observational study. *Pediatr. Res.* **87**, 940–945 (2020).

13. Ricci, F. *et al.* In vitro and in vivo characterization of poractant alfa supplemented with budesonide for safe and effective intratracheal administration. *Pediatr. Res.* **82**, 1056–1063 (2017).

14. Tashkin, D. P., Lipworth, B. & Brattsand, R. Benefit:Risk Profile of Budesonide in Obstructive Airways Disease. *Drugs* **79**, 1757–1775 (2019).

15. Waters, R. C. & Hochhaus, G. Characterization of a dextran-budesonide prodrug for inhalation therapy. *Eur. J. Pharm. Sci.* **129**, 58–67 (2019).

16. Shen, W. *et al.* SR9009 induces a REV-ERB dependent anti-small-cell lung cancer effect through inhibition of autophagy. *Theranostics* **10**, 4466–4480 (2020).

17. Durrington, H. J. *et al.* Circadian asthma airway responses are gated by REV-ERBα. *Eur. Respir. J.* **56**, 1–13 (2020).

18. Sundar, I. K., Rashid, K., Sellix, M. T. & Rahman, I. The nuclear receptor and clock gene REV-ERBα regulates cigarette smoke-induced lung inflammation. *Biochem. Biophys. Res. Commun.* **493**, 1390–1395 (2017).

19. Gindele, J. A. *et al.* Intermittent exposure to whole cigarette smoke alters the differentiation of primary small airway epithelial cells in the air-liquid interface culture. *Sci. Rep.* **10**, 1–17 (2020).

20. Munir, R., Lisec, J., Swinnen, J. V. & Zaidi, N. Lipid metabolism in cancer cells under metabolic stress. *Br. J. Cancer* **120**, 1090–1098 (2019).

21. Gao, X. *et al.* Acetate functions as an epigenetic metabolite to promote lipid synthesis under hypoxia. *Nat. Commun.* **7**, (2016).

22. Whyte, M. P. *et al.* Hypophosphatemic osteosclerosis, hyperostosis, and enthesopathy associated with novel homozygous mutations of DMP1 encoding dentin matrix protein 1 and SPP1 encoding osteopontin: The first digenic SIBLING protein osteopathy? *Bone* **132**, 115190 (2020).

23. Shintani, S. *et al.* Identification and characterization of integrin-binding sialoprotein (IBSP) genes in reptile and amphibian. *Gene* **424**, 11–17 (2008).

24. Zhang, L. *et al.* Predictive significance of bone sialoprotein and osteopontin for bone metastases in resected Chinese non-small-cell lung cancer patients: A large cohort retrospective study. *Lung Cancer* **67**, 114–119 (2010).

25. Guo, X. *et al.* Leptin signaling in intestinal epithelium mediates resistance to enteric infection by Entamoeba histolytica. *Mucosal Immunol.* **4**, 294–303 (2011).

26. Daniel E Shumer, N. J. N. N. P. S. Leptin receptor polymorphisms and lung function decline in COPD. *Physiol. Behav.* **176**, 139–148 (2017).

27. Lee, K., Lee, S. H. & Kim, T. H. The biology of prostaglandins and their role as a target for allergic airway disease therapy. *Int. J. Mol. Sci.* **21**, (2020).

28. Take, Y., Koizumi, S. & Nagahisa, A. Prostaglandin E Receptor 4 Antagonist in Cancer Immunotherapy: Mechanisms of Action. *Front. Immunol.* **11**, 1–7 (2020).

29. Dey, I., Lejeune, M. & Chadee, K. Prostaglandin E 2 receptor distribution and function in the gastrointestinal tract. *Br. J. Pharmacol.* **149**, 611–623 (2006).

30. Markovič, T., Jakopin, Ž., Dolenc, M. S. & Mlinarič-Raščan, I. Structural features of subtype-selective EP receptor modulators. *Drug Discov. Today* **22**,

721 57–71 (2017).

722 31. Nunez, F. J. *et al.* Agonist-specific desensitization of PGE2-stimulated cAMP
723 signaling due to upregulated phosphodiesterase expression in human lung
724 fibroblasts. *Naunyn. Schmiedebergs. Arch. Pharmacol.* **393**, 843–856 (2020).

725 32. Tilley, S. L. *et al.* Receptors and pathways mediating the effects of
726 prostaglandin E2 on airway tone. *Am. J. Physiol. - Lung Cell. Mol. Physiol.*
727 **284**, 599–606 (2003).

728 33. Buckley, J. *et al.* EP4 receptor as a new target for bronchodilator therapy.
729 *Thorax* **66**, 1029–1035 (2011).

730 34. Birrell, M. A. *et al.* Anti-inflammatory effects of PGE2 in the lung: Role of the
731 EP4 receptor subtype. *Thorax* **70**, 740–747 (2015).

732 35. Wang, L. *et al.* Hemodynamic and gas exchange effects of inhaled iloprost in
733 patients with COPD and pulmonary hypertension. *Int. J. COPD* **12**, 3353–3360
734 (2017).

735 36. Zhu, Y. *et al.* A prostacyclin analogue, iloprost, protects from bleomycin-
736 induced pulmonary fibrosis in mice. *Respir. Res.* **11**, 1–12 (2010).

737 37. Gohrbandt, B. *et al.* Iloprost to improve surfactant function in porcine
738 pulmonary grafts stored for twenty-four hours in low-potassium dextran
739 solution. *J. Thorac. Cardiovasc. Surg.* **129**, 80–86 (2005).

740 38. Kim, N. *et al.* Effects of Inhaled Iloprost on Lung Mechanics and Myocardial
741 Function During One-Lung Ventilation in Chronic Obstructive Pulmonary
742 Disease Patients Combined With Poor Lung Oxygenation. *Anesth. Analg.* **130**
743 (5), 1407-1414 (2020).

744 39. Lee, S. H. *et al.* Effects of intraoperative inhaled iloprost on primary graft
745 dysfunction after lung transplantation: A retrospective single center study.

Med. **95** (27), (2016).

40. Gallardo, A. *et al.* The molecular clock protein Bmal1 regulates cell differentiation in mouse embryonic stem cells. *Life Sci. alliance* **3**, 1–12 (2020).
41. Almeida, S., Chaves, M. & Delaunay, F. Transcription-based circadian mechanism controls the duration of molecular clock states in response to signaling inputs. *J. Theor. Biol.* **484**, 1–11 (2020).
42. Braghiroli, A. *et al.* Day and night control of copd and role of pharmacotherapy: A review. *Int. J. COPD* **15**, 1269–1285 (2020).
43. Zou, X. *et al.* A Systems Biology Approach Identifies Hidden Regulatory Connections Between the Circadian and Cell-Cycle Checkpoints. *Front. Physiol.* **11**, 1–9 (2020).
44. Gaucher, J., Montellier, E. & Sassone-Corsi, P. Molecular Cogs: Interplay between Circadian Clock and Cell Cycle. *Trends Cell Biol.* **28**, 368–379 (2018).
45. Rahman, I. Antioxidant therapies in COPD. *Int. J. Chron. Obstruct. Pulmon. Dis.* **1**, 15–29 (2006).
46. Yu, D. *et al.* Rev-erbα can regulate the NF-κB/NALP3 pathway to modulate lipopolysaccharide-induced acute lung injury and inflammation. *Int. Immunopharmacol.* **73**, 312–320 (2019).
47. Wiman, K. G. & Zhivotovsky, B. Understanding cell cycle and cell death regulation provides novel weapons against human diseases. *J. Intern. Med.* **281**, 483–495 (2017).
48. Maddika, S. *et al.* Cell survival, cell death and cell cycle pathways are interconnected: Implications for cancer therapy. *Drug Resist. Updat.* **10**, 13–29 (2007).

771 49. Padgett, J. & Santos, S. D. M. From clocks to dominoes: lessons on cell cycle
772 remodelling from embryonic stem cells. *FEBS Lett.* **594**, 2031–2045 (2020).
773 50. Farshadi, E., van der Horst, G. T. J. & Chaves, I. Molecular Links between the
774 Circadian Clock and the Cell Cycle. *J. Mol. Biol.* 3515–3524 (2020).
775 51. Zepp, J. A. & Morrisey, E. E. Cellular crosstalk in the development and
776 regeneration of the respiratory system. *Nat. Rev. Mol. Cell Biol.* **20**, 551–566
777 (2019).
778 52. Almeida, S., Chaves, M. & Delaunay, F. Control of synchronization ratios in
779 clock/cell cycle coupling by growth factors and glucocorticoids. *R. Soc. Open*
780 *Sci.* **7**, (2020).
781 53. Abraham, U. *et al.* Coupling governs entrainment range of circadian clocks.
782 *Mol. Syst. Biol.* **6**, 1–13 (2010).
783 54. Kistemaker, L. E. M. *et al.* Tiotropium attenuates IL-13-induced goblet cell
784 metaplasia of human airway epithelial cells. *Thorax* **70**, 668–676 (2015).
785 55. Morrow, J. D. *et al.* Functional interactors of three genome-wide association
786 study genes are differentially expressed in severe chronic obstructive
787 pulmonary disease lung tissue. *Sci. Rep.* **7**, 1–11 (2017).
788 56. Ng-Blichfeldt, J. P. *et al.* Tgf-β activation impairs fibroblast ability to support
789 adult lung epithelial progenitor cell organoid formation. *Am. J. Physiol. - Lung*
790 *Cell. Mol. Physiol.* **317** (1), L14-L28, (2019).
791 57. Torre, D., Lachmann, A. & Ma'ayan, A. BioJupies: Automated Generation of
792 Interactive Notebooks for RNA-Seq Data Analysis in the Cloud. *Cell Syst.* **7**,
793 556-561.e3 (2018).
794